Langmuir

Article

pubs.acs.org/Langmuir

Construction and Characterization of Molecular Nonwoven Fabrics Consisting of Cross-Linked Poly(γ-methyl-L-glutamate)

Rintaro Higuchi,[†] Megumi Hirano,[†] Md. Ashaduzzaman,[‡] Neval Yilmaz,[§] Tatsunori Sumino,[†] Daisuke Kodama,[†] Sayuri Chiba,[†] Shinobu Uemura,[†] Katsuhiko Nishiyama,[†] Akihiro Ohira,[∥] Michiya Fujiki,[⊥] and Masashi Kunitake*[,†,#]

[†]Graduate School of Science and Technology, Kumamoto University, 2-39-1 Kurokami, Chuo-ku, Kumamoto 860-8555, Japan

[‡]Department of Applied Chemistry and Chemical Engineering, University of Dhaka, Dhaka 1000, Bangladesh

[§]Lipid Biology Laboratory, Advanced Science Institute, RIKEN, 2-1 Hirosawa, Wako, Saitama 351-0198, Japan

[∥]Research Institute for Ubiquitous Energy Devices, National Institute of Advanced Industrial Science and Technology (AIST), 1-8-31 Midorigaoka, Ikeda, Osaka 563-8577, Japan

[⊥]Graduate School of Materials Science, Nara Institute of Science and Technology, 8916-5 Takayama, Ikoma, Nara 630-0192, Japan

[#]JST-CREST, K's Gobancho 6F, 7, Gobancho, Chiyoda-ku, Tokyo, 102-0076 Japan

ABSTRACT: Molecular nonwoven fabrics in the form of ultrathin layer-by-layer (LbL) helical polymer films with covalent cross-linking were assembled on substrates by an alternate ester−amide exchange reaction between poly(γ-methyl L-glutamate) (PMLG) and cross-linking agent ethylene diamine or 4,4′-diamino azobenzene. The regular growth of helical monolayers without excessive adsorption and the formation of amide bonds were confirmed by ultraviolet−visible (UV−vis) spectrophotometry, quartz crystal microbalance (QCM), ellipsometry, and infrared reflection−absorption spectroscopy (IR-RAS) measurements. Nanostructures with high uniformity and ultrathin films with few defects formed by helical rod segments of PMLG were characterized by atomic force microscopy (AFM) and Kelvin probe force microscopy (KFM).

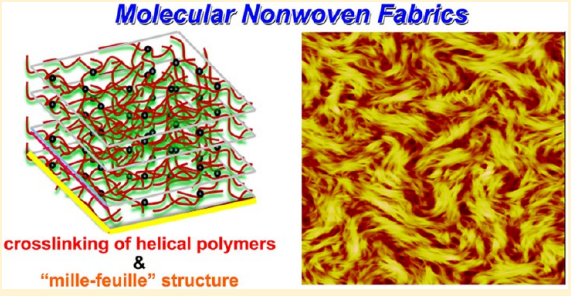

1. INTRODUCTION

During the past two decades, fundamental and commercial aspects of the construction of ultrathin films and coatings have attracted great interest. Self-assembled monolayers and spin coating and Langmuir−Blodgett methods have been utilized in the macromolecular assembly of ultrathin films. Of these methods, the layer-by-layer (LbL) assembly[1−5] technique established by Decher[1] and co-workers following the pioneering report by Iler[3] has become very popular and has been extensively used because it facilitates the preparation and control of layer structures. A large number of reports on LbL film preparation using various techniques have been published. In general, the preparation of an LbL assembly is conducted through the alternate electrostatic adsorption of oppositely charged species on a uniformly charged planar substrate. For a variety of applications, the LbL process offers great versatility for the deposition of various charged organic/inorganic materials[6,7] such as polyelectrolytes,[8−13] nanoparticles,[6] proteins,[14−16] DNA,[12,16−24] charged polysaccharides,[25−28] and even charged viruses.[13] Electrostatic interactions and noncovalent interactions such as hydrogen bonds,[29] charge-transfer complexes,[30] and stereocomplex formation[31] have been widely used to form layered structures. Industrially important polymeric multilayer films prepared by LbL are potentially suitable for a variety of applications, including drug delivery,[25,27,28,32] reversible loading and release of dyes and nanoparticles,[33] liquid crystal command layers,[34] sensors,[35−37] antireflection coatings,[38] permeability control,[39] ion selectivity,[40] dye-sensitized solar cells,[41] and optical properties.[42,43] The structures and quality of LbL films depend substantially on the experimental conditions, which have been systematically researched.[1,44−46] Moreover, LbL methodology has been extended beyond supported ultrathin films to self-supported LbL thin films,[4] hollow capsules,[47−51] and nanotubes.[52]

Although most work has been focused on the assembly of LbL films by either electrostatic or hydrogen bonding interactions, polymer multilayer assembly facilitated by covalent bonding has also been reported.[49−56] Covalent bonding significantly strengthens the assembled structure and is very advantageous for practical applications. Recently, the construction of covalent LbL films based on the click reaction,[55] which can be performed under extremely mild conditions with high reaction yields, has been reported. In addition, Cao and co-workers have reported that covalent cross-linking between

Special Issue: Interfacial Nanoarchitectonics

Received: November 15, 2012
Revised: December 20, 2012
Published: December 20, 2012

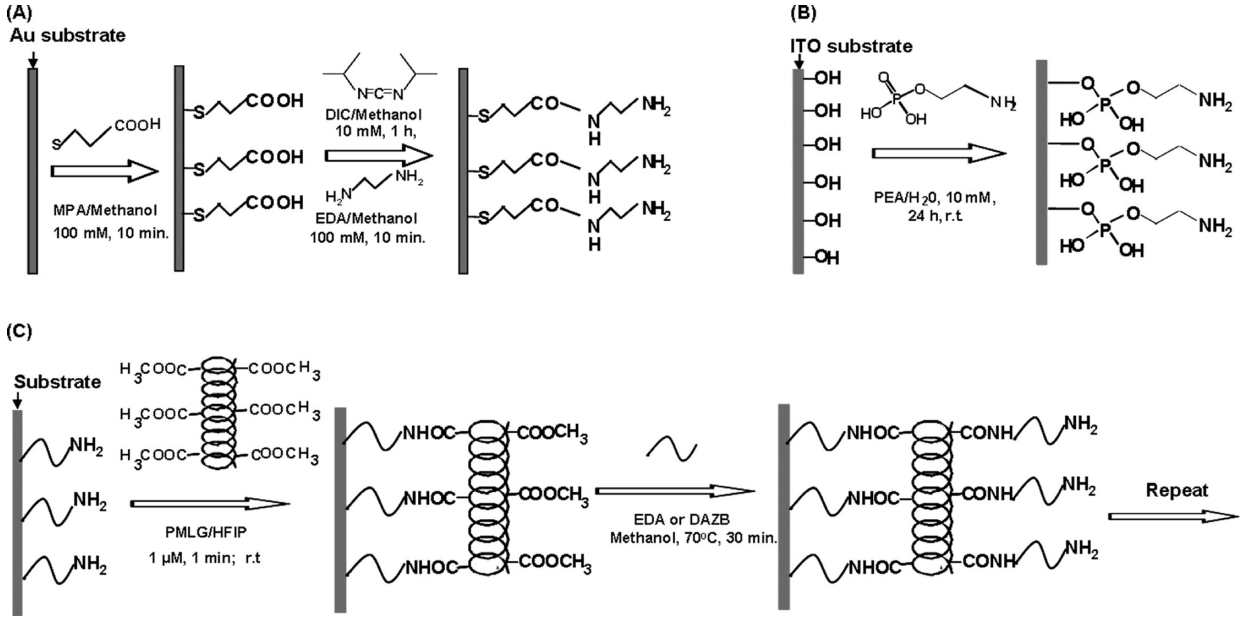

Figure 1. Reaction scheme for surface activation of (A) an Au-coated quartz substrate and (B) an ITO-coated glass substrate and (C) consecutive alternate reactions between PMLG and cross-linkers.

layers has been achieved by UV irradiation after the deposition of LbL films.[57]

LbL films of a polymer that possesses a secondary structure, α helix or β sheet, have been frequently investigated. The study of helical polymers with unique secondary structures and properties has attracting increasing interest with respect to preparing functional materials such as stimuli-responsive functional materials,[58] nanotube fabrication,[59] biomedical applications,[60] optically active materials,[61] chromatographic purification of proteins,[62] liquid crystals,[63] food, cosmetics, and pharmaceutical products.[64] LbL films containing poly(L-lysine) (PLL) and poly(L-glutamic acid) (PLGA) that exhibit secondary structure based on the peptide have been reported.[65−67] In these films, the preferred orientation of peptides in the β-sheet structures is antiparallel within sheets and parallel between sheets. In addition, a molecular dynamics study has indicated that hydrophobic interactions and electrostatic interactions play a significant role in the assemblies. Serizawa and co-workers have reported the stepwise assembly of isotactic poly(methyl methacrylate) and syndiotactic poly(methacrylic acid) on a substrate based on stereocomplex formation.[68,69]

In this article, we report the preparation of LbL ultrathin films that can be regarded as a molecular nonwoven fabric comprising poly(γ-methyl L-glutamate) (PMLG) layers with a high density of interlayer cross-links. The secondary structure of the helical polymer is advantageous for the construction of a covalently bonded ultrathin nonwoven fabric consisting of single polymer strands. PMLG is one of the most popular synthetic helical polymers and generally possesses a helical secondary structure that is regulated by intramolecular hydrogen bonds along the backbone. Jaworek et al. focused the electromechanical properties of a monomolecular helical film of poly(γ-benzyl L-glutamate) with directionally aligned nanometer-scale thickness grafted at the carboxyl-terminal end onto a flat aluminum surface.[70]

In addition to conventional analysis methodologies for ultrathin organic films such as quartz crystal microbalance (QCM) measurements, infrared reflection−absorption spectroscopy (IR-RAS), and ultraviolet−visible (UV−vis) absorption spectrophotometry, Kelvin probe force microscopy (KFM), which is derived from atomic force microscopy (AFM), was carried out to elucidate the nanostructure of the molecular nonwoven fabric. The KFM technique[71] provides surface potential mapping of deposited films on the submicrometer scale. Since its invention in 1991 as a fusion of AFM and the Kelvin probe technique,[72,73] KFM has been applied to the surface mapping of the work function, which relates to many surface phenomena such as catalytic activity[71] and the doping and band bending of semiconductors.[75,76] Moreover, KFM has also been applied to organic materials such as heterojunction organic solar cells,[77,78] carbon nanomaterials (carbon fibers and graphene),[79] DNA, and proteins.[80]

2. EXPERIMENTAL SECTION

Materials and Methods. Poly(γ-methyl L-glutamate) (PMLG1000, Dp = ca.1000, Ajicoat A-2000, Ajinomoto. Co. Inc., Japan, molecular weight (M_w) = 117 000 g mol^{-1}, in ethylene dichloride solution) was supplied by Ajinomoto Co. Ltd. Japan. Other samples of PMLG with lower M_w (PMLG100, Dp = 100; PMLG4, Dp = 4) were purchased from GenScript Corporation, USA. All PMLG samples were used without further purification. All other reagents were also used as received. 1,1,1,3,3,3-Hexafluoroisopropanol (HFIP, 99.0%), ethylenediamine (EDA, 99.5%), *N*,*N*′-diisopropylcarbodiimide (DIC, 99%), and 2-aminoethyldihydrogenphosphate (PEA) were purchased from Wako Pure Chemical Industries Ltd. Other chemicals used were 4,4′-diaminoazobenzene (DAZB, 95%, Alfa Aesar, Ward Hill, MA, USA) and 3-mercaptopropionic acid (MPA, Nacalai Tesque). An Au-deposited quartz crystal resonator (AT cut, 9 MHz, USI Co. Ltd., Fukuoka Japan), "rough" indium tin oxide (ITO)-coated glass (Koshi Optical Industry Co. Ltd., Japan), and "flat" polished ITO-coated glass (Kuramoto Co. Ltd. Japan) were used as substrates.

Surface Activation. For both Au-coated quartz crystal and ITO-coated glass substrates, the alternate deposition procedures were essentially the same but the surface activation procedure depended on the type of substrate, as shown in Figure 1. After being rinsed with acetone, Au-deposited quartz crystals were etched with piranha solution (70:30 sulfuric acid/H_2O_2) and thoroughly rinsed with pure water and pure methanol prior to use. Piranha solution is an irritant

dx.doi.org/10.1021/la3045576 | *Langmuir* 2013, 29, 7478−7487

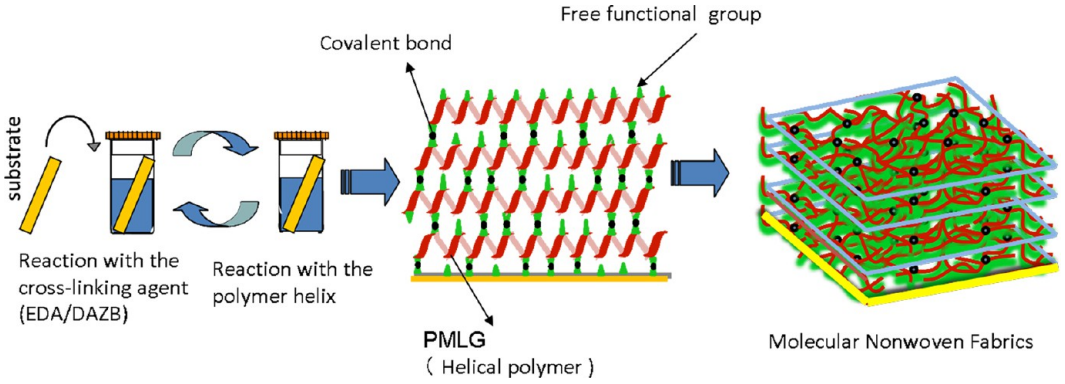

Figure 2. Schematic representation of the methodology used to construct molecular nonwoven fabrics consisting of a helical polymer on a substrate by an alternate reaction through chemical bonding between the ester groups of the polymer helix and the amino groups of the cross-linking agent.

and requires careful handling. The clean gold-coated plates were dipped into a 100 mM methanolic solution of MPA for about 10 min. The substrates were then immersed in a methanolic solution of 10 mM DIC for 60 min followed by dipping in 100 mM methanolic EDA solution (Figure 1A). MPA on the surface was reacted with EDA using the condensation agent DIC to convert the terminal units.

Two rough, flat ITO-coated glass plates with different roughnesses were used to compare the influence of surface roughness on the deposition behavior and morphology of the deposited films. An ITO-coated glass plate was cut into 50 × 10 mm^2 pieces and washed with a detergent with sonication for about 30 min. The substrate was then sonicated several times with deionized water to remove adhered detergent, rinsed with copious amounts of water, and dried with compressed N_2 before use. The ITO-coated glass substrate was modified by the immersion of clean substrates in a 10 mM aqueous solution of PEA for 24 h, followed by rinsing with pure water (Figure 1B).

Multilayer Growth. A typical procedure for the alternate LbL deposition of PMLG is shown in Figure 1C. In the PMLG modification step, the pretreated substrates bearing primary amino units were immersed in HFIP solution containing PMLG (typically 3.6 mg in 25 mL) at room temperature for 1 min, rinsed with either 1,2-dichloroethane (EDC) or HFIP, and again dipped into the respective solvent for another minute. To effect the next step of modification with cross-linker, the samples with adsorbed PMLG were immersed in a methanolic solution of 5 mM cross-linker (EDA or DAZB) at room temperature or 70 °C for 30 min and then rinsed with pure methanol. Compared to the reaction with PMLG, more severe conditions were used for the reaction with EDA to achieve complete replacement of the ester on PMLG with an amide. After each step, the sample was immediately dried in a nitrogen gas stream. After the formation of a designated number of PMLG layers, the substrates were subjected to instrumental analysis.

Layer Growth Analysis. Layer growth of PMLG LbL films was monitored by QCM and UV−vis. QCM measurements were carried out on each sample after PMLG deposition. Prior to QCM measurement, the LbL-deposited samples were thoroughly rinsed and dried. QCM (9 MHz) was applied to analyze the assembly quantitatively; the frequency was monitored with an Iwatsu frequency counter (model SC-7201). The amount of polymer bonded, Δm (ng), was estimated by measuring the frequency shift, ΔF (Hz), using Sauerbrey's equation:

$$-\Delta F = \frac{2F_0^2}{A\sqrt{\rho_q \mu_q}}\Delta m \quad (1)$$

$$C_{\mathrm{PMLG\ unit}} = \frac{\Delta m_{av}}{M_{\mathrm{PMLG\ unit}}} \times \frac{N_A}{A} \quad (2)$$

F_0 is the parent frequency of the QCM (9 × 10^6 Hz), A is the electrode area (0.16 cm^2), ρ_q is the density of the quartz (2.65 g cm^{-3}), and μ_q is the shear modulus (3.78 × 10^{11} dyn cm^{-2}). $C_{\mathrm{PMLG\ unit}}$ is the surface concentration (average number of repeating molecular units of PMLG, molecular unit nm^{-2}), Δm_{av} is the average polymer mass increase in the PMLG deposition step, $M_{\mathrm{PMLG\ unit}}$ is the unit molecular weight of PMLG, and N_A is Avogadro's constant. Equation 1 was reliable when measurements were performed under a stream of N_2 gas.

The deposition behavior of PMLG-DAZB films on rough ITO-coated glass was also monitored by UV−vis spectrometry (Jasco V-650). According to eq 3, on the basis of Lambert−Beer's law, the average surface concentration of DAZB units was estimated from the absorbance at 400 nm, which is attributed to azo chromophore units.

$$\mathrm{Abs} = \Sigma_{\mathrm{DAZB}}(\mathrm{cm^2/mol}) \times D(\mathrm{mol/cm^3}) \times 1\ \mathrm{cm} = \varepsilon_{\mathrm{DAZB}}(\mathrm{cm^2/mol}) \times \mathrm{D(mol/cm^2)} \quad (3)$$

Spectroscopic Ellipsometry. The thickness of the layers of PMLG-DAZB and PMLG-EDA deposited on a flat ITO was measured by ellipsometry (Ohtsuka Denshi, Fe-5000S, Japan). The T-Lorentz-n fitting model was used for thickness analysis. Because the PMLG-Azo films exhibit UV−vis adsorption, the t-Lorentz-n equation was used to determine film thicknesses from ellipsometric data. The fitting parameters are A = 30, C = 0.7, and E_0 = 5 as the first term and A = 20, C = 0.5, and E_0 = 3 as the second term. E_g and e are 2.8 and 1.55, respectively. Here, A is the amplitude of the Lorentz function, C is the half bandwidth, E_0 is central wavelength, E_g is the absorption end, and e is the refractive index.

IR-RAS Measurements of the PMLG LbL Films. IR-RAS of multilayer films on ITO-coated glass substrates was conducted with an FT-IR spectrometer (Bio-Rad, FTS-6000) with a high sensitivity reflection unit (Refractor2, Harrick Scientific). Spectra (4000−600 cm^{-1}) were collected at 4 cm^{-1} resolution using 32 scans under ambient conditions. To confirm the formation of amide bonds, IR-RAS was also performed on a sample that was assembled on a piece of Au-coated mica in 10 cycles (EDA/PMLG).

AFM/KFM Observation. AFM images were recorded with a NanoScope IIIa (Digital Instruments, Inc.) equipped with an E scanner in tapping mode and an Agilent 5500 AFM/SPM in AAC (Acoustic ac) mode in air under ambient conditions. A commercial silicon cantilever was used as an ordinary AFM tip (e.g., Veeco Instruments, MPP-11100, resonance frequency ≈ 300 kHz, and spring constant ≈ 40 N/m).

KFM was conducted with an Agilent 5500 (Agilent Technologies, Inc.) and a conductive $PtIr_5$-doped silicon cantilever (Nanoworld R&D, PPP-EFM, resonance frequency ≈7 5 kHz and average spring constant ≈ 2.8 N/m). The polymer-coated ITO substrates were grounded, and the bias voltage (1 V) was applied to the cantilever.

3. RESULTS AND DISCUSSION

Alternate Deposition of PMLG Polymer Films Cross-Linked with Linker Molecules. Covalent alternate deposition of PMLG was performed by the ester−amide exchange

dx.doi.org/10.1021/la3045576 | Langmuir 2013, 29, 7478−7487

reaction between ester groups on PMLG and a primary amino group on cross-linker molecules (EDA and DAZB), Au-coated quartz crystals, and ITO-coated glass substrates as presented schematically in Figure 2. Prior to starting the consecutive deposition of PMLG, primary amino groups were introduced onto the substrates as a bridgehead for LbL deposition. An alternate LbL reaction was conducted by alternate immersion in PMLG solution and linker solution. Ester groups in PMLG reacted with primary amino groups introduced onto substrates to deposit a PMLG layer. The PMLG surface was then reacted with a cross-linker molecule bearing two primary amino groups to reproduce primary amino groups on the surface for the next LbL reaction with PMLG. The application reaction was similar to the ester−amide exchange reaction, which is frequently used for the synthesis of amidoamine-type dendrimers.[81]

Alternate Deposition Monitored by QCM. Regular LbL growth of helical monolayers on a gold substrate was confirmed by QCM. Figure 3 shows the typical deposition behavior of

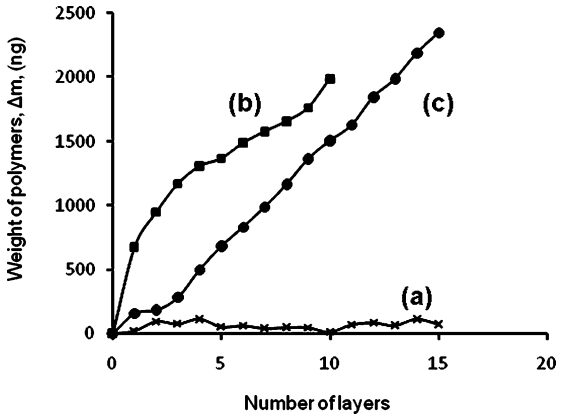

Figure 3. Plots of the amount deposited vs the number of PMLG-EDA LbL layers for the alternate reaction of (a) 250 μM PMLG4, (b) 10 μM PMLG100, and (c) 1 μM PMLG1000 on Au-coated QCM at room temperature. HFIP was used for rinsing. Data were obtained after bonding PMLG polymers onto the substrate surface in each reaction cycle.

PMLG-EDA LbL films monitored by QCM. LbL deposition using PMLG4 (with Dp = 4) gave no QCM increment, and hence only a small amount of the polymer was deposited. By contrast, the LbL deposition of PMLG100 and PMLG1000 was an almost constant in each step. Although the deposition weight in the first reaction with PMLG onto the pretreated substrate tended to be less reproducible, the subsequent average increments of the amount deposited were constant with high reproducibility. The scattered values in the first PMLG introduction might be due to the uncontrolled surface roughness. In each deposition cycle, the weight increments in the PMLG deposition steps were always apparent, but in the reaction step with cross-linker, definite mass increments were observed for neither EDA nor DAZB. In the case of PMLG1000, the average $-\Delta F$ values for reaction with EDA and PMLG were 11 and 165 Hz for one cycle with EDA and PMLG, respectively. Reactions with both EDA and PMLG spontaneously terminated, giving a highly reproducible film thickness growth step that demonstrates the reproducibility of the stable formation of LbL films. The surface concentration (the average number of PMLG repeat units) for each PMLG deposition cycle was estimated to be roughly 4.4 molecular units nm^{-2} $layer^{-1}$ (the occupied area, 0.23 nm^2 molecular $unit^{-1}$ $layer^{-1}$). The small, constant polymer mass increase in the PMLG reaction step suggests the monolayer-by-monolayer assembly of PMLG films.

In general, for LbL film growth between polycations and polyanions a high concentration of polyions is necessary to affect alternate adsorption because the excess adsorbate in every step requires resaturation for the subsequent step. Consequently, the thicknesses of the polymer layers in such LbL films are not to molecular scale, although the thickness is very reproducible for every step. The films formed in our experiments were suspended by one-by-one amide bond formation in a small-concentration solution. However, the use of a rigid helical polymer such as PMLG allowed molecular-level assembly and an alternate reaction from small-concentration solutions without excess adsorption. Fresh unconnected functional units for the next reaction were always kept on the solution side of the films because of the rigid cylindrical structure of helical polymers (Figure 2). The fact that short-chain PMLG4 gave no LbL deposition proves that a helical secondary structure is necessary for constant alternate deposition. PMLG4 is too short to possess a stable helical conformation because the helical pitch of PMLG is 0.54 nm.

Alternate Deposition Monitored by UV−Vis Spectroscopy. The deposition behavior of ultrathin layers of PMLG1000 cross-linked with DAZB on ITO glass substrates was also studied by monitoring the absorbance of azo chromophore units from DAZB. UV−vis spectra are shown in Figure 4a, and the corresponding absorbances at 400 nm for

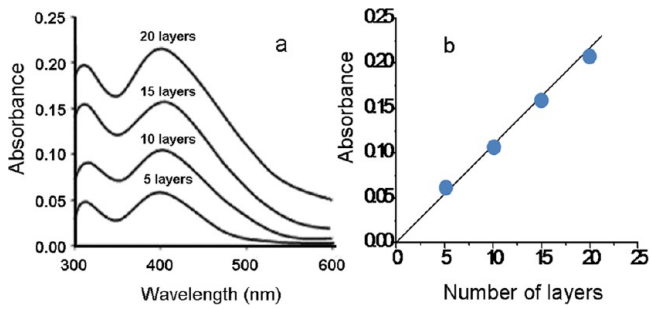

Figure 4. (a) UV−vis spectra and (b, inset) the corresponding plots of absorbance at 400 nm for PMLG1000-DAZB films on rough ITO-coated glass substrates.

PMLG-DAZB films are plotted against the number of layers in Figure 4b. The plot shows a constant rate of increase of absorbance with an increasing number of layers, indicating that a regular, stable deposition of PMLG layers was achieved. Thus, a constant number of DAZB molecules reacted with PMLG in each layer.

The average surface concentration of azo units in each layer calculated from the slope of the absorbance versus the number of layers graph was 8.36×10^{-10} mol cm^{-2} $layer^{-1}$, which corresponds to the apparent occupied area of 0.199 nm^2 $(DAZB\ molecule)^{-1}$ $layer^{-1}$. This value roughly matched the surface concentration of PMLG repeat units obtained by QCM in order of magnitude. The linearity of LbL deposition was also confirmed by spectroscopic ellipsometry of up to 30 layers, as shown in Figure 5. The average layer thickness was roughly 5 nm for both DAZB-PMLG and EDA-PMLG, which is larger than the expected diameter (1.2 nm) of the PMLG helix.[82,83]

dx.doi.org/10.1021/la3045576 | Langmuir 2013, 29, 7478−7487

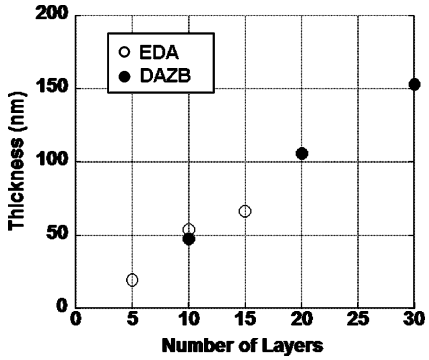

Figure 5. Layer thickness monitored by spectroscopic ellipsometry for PMLG1000-DAZB films on ITO-coated glass substrates versus the number of PMLG layers.

The discrepancy might be due to the partial entanglement of PMLG chains on the surface.

Confirmation of Bond Formation by IR-RAS. The constant rate of growth of films and high stability of the films in organic solvents strongly suggest a highly cross-linked structure between helical polymer layers. To confirm the formation of amide cross-links between layers and the preservation of the α-helix conformation in LbL films, IR-RAS measurements were conducted. Figure 6 shows typical IR-RAS spectra for a PMLG film (PMLG1000-EDA, five cycles, terminated by PMLG) on an Au-coated plate and native PMLG. Native PMLG (Figure 6B) produced vibrations of ester and amide units that were observed at 1232 and 1283 cm^{-1} and 1550 and 1651 cm^{-1}, respectively. Deposited PMLG was in the α-helical conformation, as demonstrated by the spectral positions of the amide I (1651 cm^{-1}) and amide II (1550 cm^{-1}) absorption bands.[70] In the case of the PMLG-LbL films, the signal of the ester unit was significantly decreased by the ester−amide exchange reaction in comparison to those of the amide unit. The results indicate that most of the ester units reacted with cross-linker molecules and changed to amide groups.

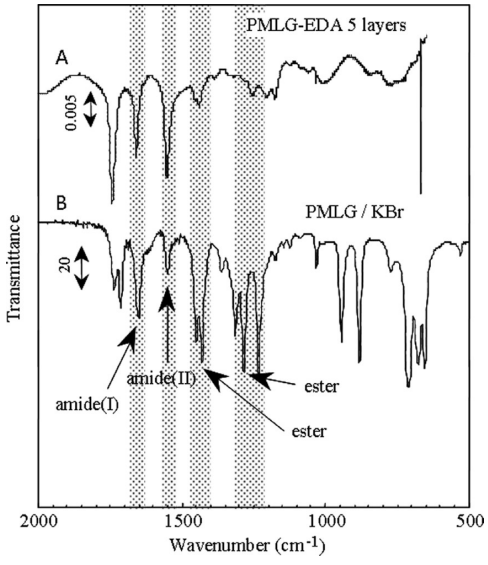

Figure 6. Typical IR-RAS spectra of (A) a layered PMLG1000-EDA polymer film (five PMLG layers) assembled on Au-coated mica and (B) PMLG (KBr method).

AFM Observation of the Surface Morphology Dependence on the Number of Layers. The surface morphologies of the polymer films on ITO glass substrates were investigated by AFM imaging. To elucidate the morphology change in the cycles of deposition, PMLG1000-EDA films were prepared on a special flat ITO surface with corrugations less than several nanometers deep. Figure 7a shows a typical AFM image of individual PMLG polymer rods on the flat ITO, prepared by the single-cycle deposition of PMLG and rinsing with HFIP. Individual helical polymer chains were clearly recognized on the long-range micrometer-scale undulation of the ITO substrate. The AFM-measured height and width of the single PMLG chains were roughly 1.2 and 40 nm, respectively. Although the height was similar to the

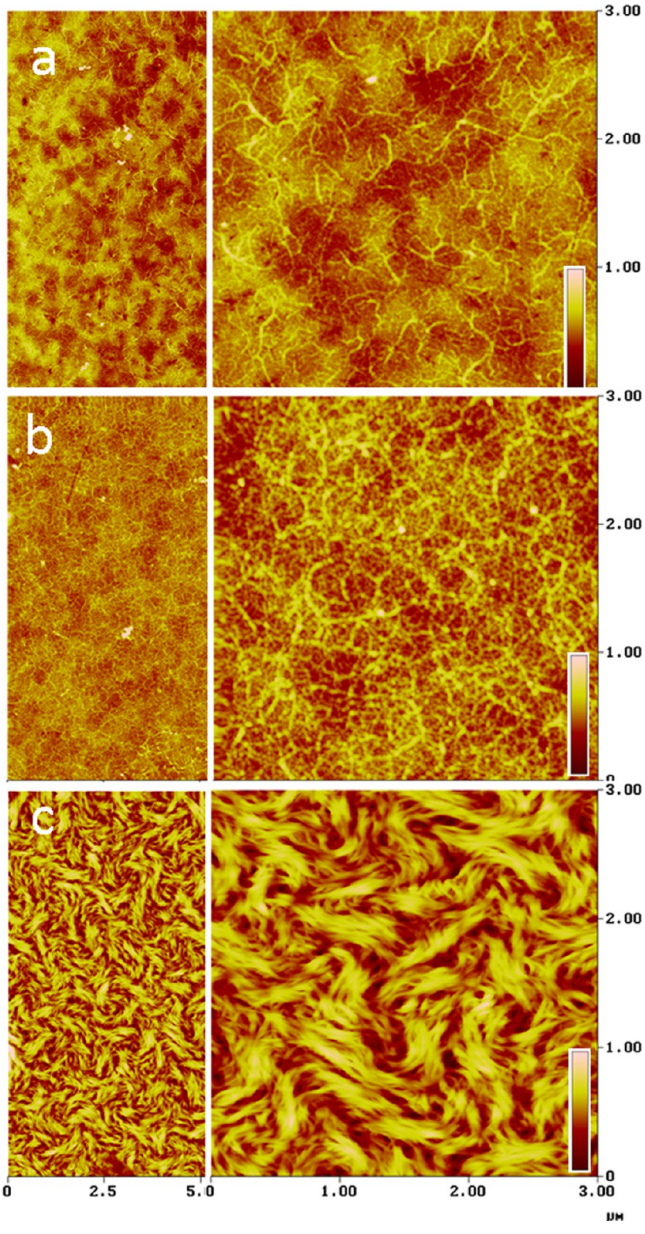

Figure 7. AFM tapping-mode topographic images of PMLG1000-EDA LbL films. (a) 1 layer, (b) 5 layers, and (c) 20 layers on flat ITO glass with wide (left) and narrow (right) scales. The sample was rinsed with HFIP. The insets on the right-hand side show height indicators for (a) 20, (b) 30, and (c) 100 nm. The height indicator is 100 nm full scale.

dx.doi.org/10.1021/la3045576 | Langmuir 2013, 29, 7478−7487

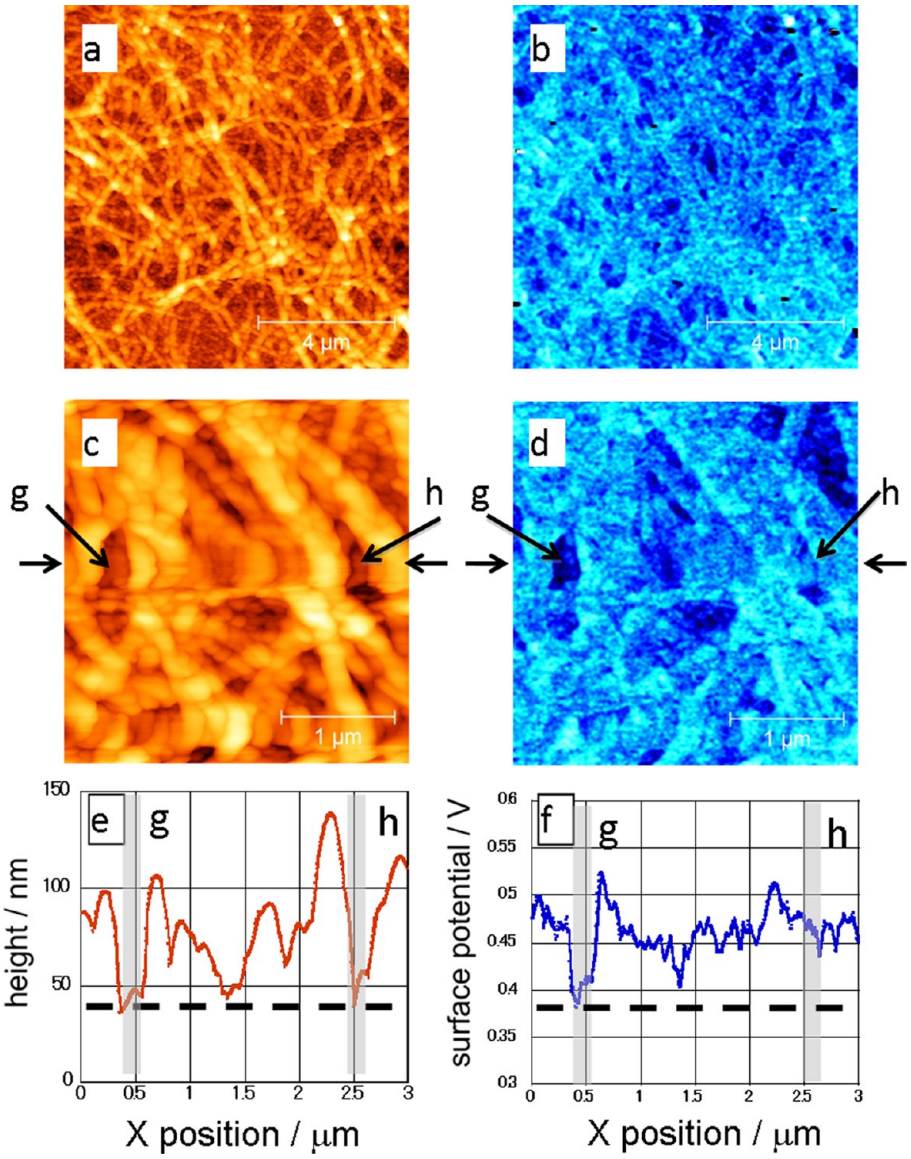

Figure 8. Topographic (AFM; a, c, e) and surface potential (KFM; b, d, f) images of PMLG1000-EDA LbL films with five PMLG multilayers on ITO-coated glass prepared by rinsing with EDC.

real diameter of α-helical PMLG (1.20 nm),[82,83] the width might have reflected the radius of curvature of the AFM tip.

PMLG strings were scattered and partially connected to each other over the surface in a meshlike assembly. After five cycles of PMLG deposition, a PMLG network structure had grown and uniformly covered the whole surface so that the underlying substrate could not be observed (Figure 7b). Helical polymer strings were folded and adhered to form a nanostructured nonwoven fabric consisting of single molecular strands. Twenty cycle films revealed the beautiful texture shown in Figure 7c. The twisted feature indicates that it was produced by the hierarchical helical bundle aggregation of helical polymers with high uniformity. The same texture was observed for more than 20 PMLG thin films with high reproducibility on both flat and rough ITO-coated glass. The average increment of film thickness measured by ellipsometry (ca. 5 nm) was larger than the expected diameter of helical PMLG (1.2 nm), although the QCM results suggest monolayer-by-monolayer assembly. These results indicate that PMLG helices possess a network structure based on the 3-D entanglement of PMLGs, not close hexagonal packing. The AFM images of the textilelike feature strongly support this idea. The formation of a bundle of peptides in polyelectrolyte LbL has been reported by Zhang and co-workers.[84]

Despite essentially no difference in the surface morphology of the PMLG films between EDA and DAZB systems, it was significantly affected by the solvent used for rinsing. When EDC was used as the rinsing solvent instead of HFIP, a very different morphology was observed. Figure 8a,c shows topographic images (AFM) of five layered PMLG1000-EDA LbL films on flat ITO-coated glass prepared by rinsing with EDC solvent. A rough network structure consisting of larger bundles of strings was regularly observed for fifth cycle PMLG deposition. In the enlarged image in Figure 8c, larger bundles with an apparent diameter of 50−150 nm appear, rather than the structures that resulted from rinsing with HFIP. The difference is due to the relatively poor solubility of PMLG in EDC compared to that in HFIP. Rinsing with EDC after the deposition of PMLG in HFIP solution may induce the aggregation of PMLG and the growth of bundles with

dx.doi.org/10.1021/la3045576 | Langmuir 2013, 29, 7478−7487

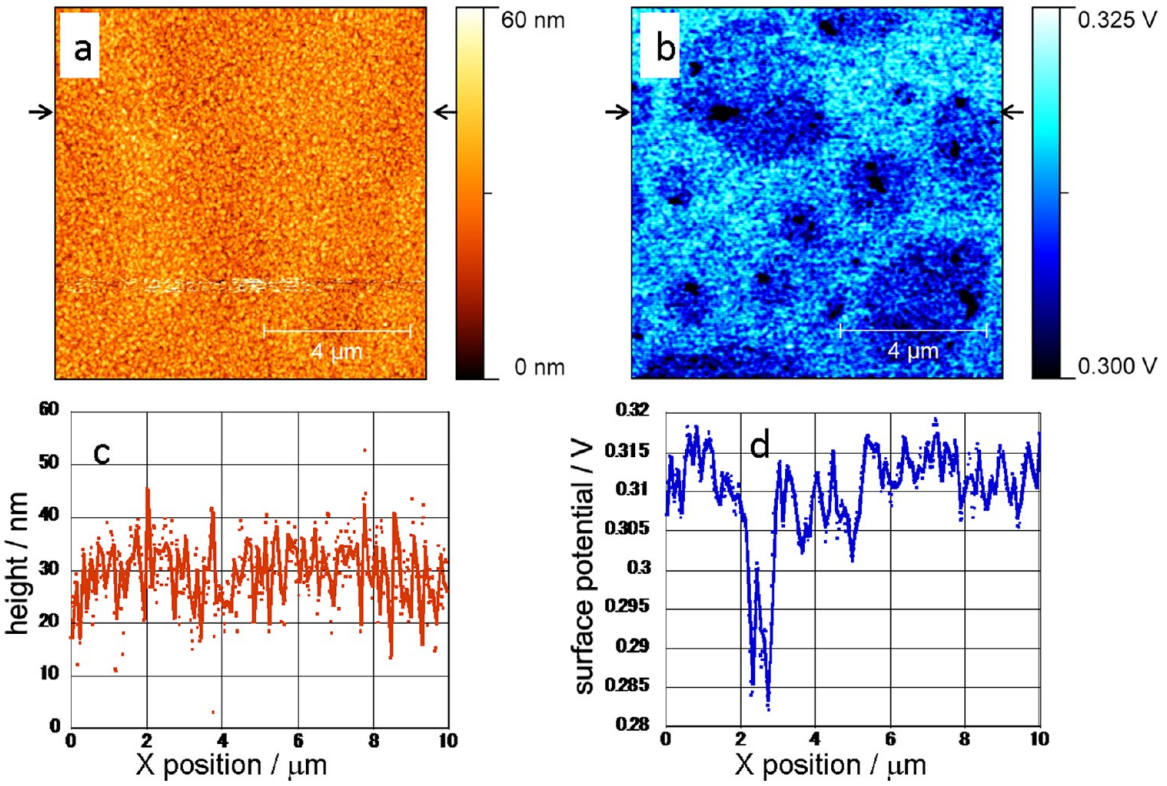

Figure 9. Topographic (AFM, a) and surface potential (KFM, b) images of PMLG1000-DAZB LbL films (5 PMLG multilayer) on rough ITO-coated glass prepared by rinsing with HFIP solvent and the corresponding cross sections (c, d) at the line marked by the arrows.

unreacted PMLG molecules on the surface. In addition, structural changes in polyelectrolyte LbL films based on salt rinsing has been reported recently.[85,86]

KFM Observation of the PMLG LbL Films. Surface potential mapping with KFM, in addition to AFM, was used to observe PMLG LbL films on the submicrometer scale. Figure 8b,d shows KFM surface potential images that correspond to the AFM images in Figure 8a,c, respectively. Similar to that shown by the topographic images, a segregated bundle structure was observed in the KFM images. The contrast of the bundle network structure in the KFM image seems to be reflected in the topographic features rather than the difference in surface potential. The obvious difference between AFM and KFM was frequently observed in valleys located between bundles. As a typical example, the two deep valley points g and h were marked with arrows in both images and lines in the cross sections. The depths of the valleys observed from the AFM image were essentially the same and roughly 40 nm. However, the KFM images at corresponding points g and h revealed a difference in the surface potential.

The surface potential at point g was 0.056 V more negative than the value at the point marked by the arrow, h, probably indicating that locations g and h corresponded to a bare negative ITO surface and cationic PMLG-coated areas, respectively. KFM achieved imaging of defects based on differences in surface potential, although it might be very difficult to eliminate topographic information from KFM images to emphasize surface potential information. In the case of the finer helical polymer mesh structured films (Figure 7), there was no significant difference between AFM and KFM images because of the limited resolution of KFM.

As noted previously, the morphology of PMLG with less than five layers was not visualized on rough ITO-coated glass because the polymer morphology was masked by the larger-scale corrugations of the substrate. Surprisingly, KFM revealed a higher potential for visualizing the defects of the polymer films on a rough surface but not on a flat surface, in contrast to AFM. Figure 9 shows a comparison of a topographic (AFM) image and the corresponding surface potential (KFM) image of five-layered PMLG-DAZB LbL films deposited on rough ITO-coated glass prepared by rinsing with HFIP. To minimize topographic information, the PMLG films deposited on the substrate were compared in AFM/KFM imaging.

The surface morphology of PMLG films on rough ITO observed in Figure 9a consisted of protrusions on a scale of several tens of nanometers. The roughness was originally from the morphology of the substrate, spattered ITO on glass itself, rather than deposited PMLG layers. No information about the surface morphology of PMLG could be obtained. However, the corresponding KFM image showed several dark points with surrounding pigmented areas on the micrometer scale. The average surface potentials for the dark points, pigmented areas, and other areas were 0.29, 0.30, and 0.31 V, respectively. The points with lowest surface potential, ca. 0.29 V, are attributed to point defects of the PMLG films, and the brightest area with higher surface potential, typically 0.31 V, is an area that was covered by LbL films. In the thicker PMLG films with more than 20 PMLG layers, AFM showed typical features of a PMLG mesh (Figure 7c) and KFM showed similar features but with lower resolution.

The local surface potential measured by KFM would be very significant for organic materials. However, it is not easy and simple in terms of reproducibility and reliability, probably because of tip contamination and the deconvolution of topographic information. In rare cases, a contrast-reversed KFM image was obtained, which is thought to be due to a

dx.doi.org/10.1021/la3045576 | Langmuir 2013, 29, 7478−7487

contaminated tip. To avoid the contamination problem, the tips were checked with standard samples before and after imaging. Highly oriented pyrolytic graphite (HOPG) and intact ITO were used as standard surface samples and gave −0.16 ± 0.01 and 0.00 ± 0.03 V, respectively, as standard surface potentials. When the surface potential of HOPG was slightly shifted, the value was compensated to zero and then the surface potential difference between HOPG and ITO was confirmed. Tips that gave different surface potentials for the standards were not used for further experiments.

Figure 10 shows the variation of surface potential with the number of PMLG layers. The initial surface potentials observed

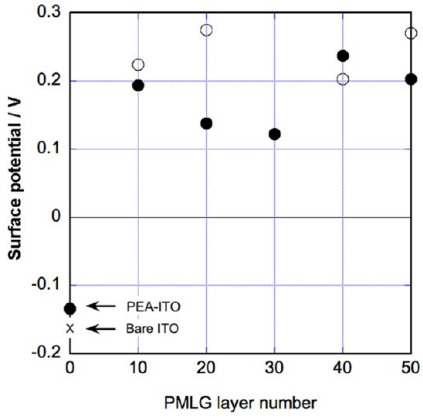

Figure 10. Plots of the surface potential of PMLG1000-EDA (○) and PMLG1000-DAZB (●) films vs the number of PMLG layers.

for intact ITO and modified ITO were typically −0.16 and −0.15 V, respectively. The surface potentials increased with the number of PMLG layers and eventually became approximately constant at ca. +0.25 V for 30 PMLG layers. The positive values are due to free amino units introduced via the EDA cross-linker. Compared to EDA, the PMLG-DAZB system gave slightly smaller surface potentials. The surface potential of PMLG-terminated surfaces (with 10 PMLG layers) was 0.2 ± 0.1 V, and there was no significant difference between PMLG-terminated and cross-linker-terminated surfaces. The results indicate that KFM sensed surface potential information not only from the surfaces but also from below the surface of the materials. The surface potentials of PMLG-terminated surfaces were relatively scattered compared to the surface potentials of cross-linker-terminated surfaces.

4. CONCLUSIONS

The facile methodology that was developed for monolayer-by-monolayer ultrathin polymer films comprised the formation of single helical PMLG monolayers attached to the substrate surface that were covalently cross-linked. The results of QCM, UV−vis spectroscopy, and scanning probe techniques clearly demonstrated uniform ultrathin films prepared by regular LbL growth with thickness corresponding to the diameter of the helical polymer chains. The rigidity of the secondary helical structure of PMLG allowed us to keep reactive groups on the surface for the next reaction cycle. This covalently cross-linked ultrathin film, effectively a molecular nonwoven fabric consisting of a helical polymer, is very interesting in terms of strength and insolubility. We believe that this approach will provide a route to the construction of highly cross-linked ultrathin films of poly(amino acid)s with molecular-level architecture. In addition, KFM was demonstrated to be a powerful tool for the investigation of polymeric materials.

AUTHOR INFORMATION

Corresponding Author

*E-mail: kunitake@kumamoto-u.ac.jp.

Author Contributions

This article was written through the contributions of all authors, and all authors have given approval to the final version of the article.

Notes

The authors declare no competing financial interest.

ACKNOWLEDGMENTS

This work was partially financially supported by the Ministry of Education, Science, Sports, and Culture of Japan. We are deeply indebted to Ajinomoto Co. Ltd. Japan, which supplied high-molecular-weight PMLG. This work was partially supported by a Grant-in-Aid for Scientific Research on Innovative Areas "New Polymeric Materials Based on Element-Blocks" (24102006) of the Ministry of Education, Culture, Sports, Science, and Technology, Japan.

REFERENCES

(1) Decher, G. Fuzzy nanoassemblies: toward layered polymeric multicomposites. *Science* **1997**, *277*, 1232−1237.
(2) Ariga, K.; Hill, J. P.; Ji, Q. Layer-by-layer assembly as a versatile bottom-up nanofabrication technique for exploratory research and realistic application. *Phys. Chem. Chem. Phys.* **2007**, *9*, 2319−2340.
(3) Iler, R. K. Multilayers of colloidal particles. *Colloid Interface Sci.* **1966**, *21*, 569−594.
(4) Vendamme, R.; Onoue, S.-Y.; Nakao, A.; Kunitake, T. Robust free-standing nanomembranes of organic/inorganic interpenetrating networks. *Nat. Mater.* **2006**, *5*, 484−501.
(5) Bergbreiter, D. E.; Liao, K.-S. Covalent layer-by-layer assembly - an effective, forgiving way to construct functional robust ultrathin films and nanocomposites. *Soft Matter* **2009**, *5*, 23−28.
(6) Hao, E.; Lian, T. Layer-by-layer assembly of CdSe nanoparticles based on hydrogen bonding. *Langmuir* **2000**, *16*, 7879−7881.
(7) Kim, J.-H.; Fujita, S.; Shiratori, S. Fabrication and characterization of TiO_2 thin film prepared by a layer-by-layer self-assembly method. *Thin Solid Films* **2006**, *499*, 83−89.
(8) Porcel, C.; Lavalle, Ph.; Decher, G.; Senger, B.; Voegel, J.-C.; Schaaf, P. Influence of the polyelectrolyte molecular weight on exponentially growing multilayer films in the linear regime. *Langmuir* **2007**, *23*, 1898−1904.
(9) Michel, M.; Izquierdo, A.; Decher, G.; Voegel, J.-C.; Schaaf, P.; Ball, V. Layer by layer self-assembled polyelectrolyte multilayers with embedded phospholipid vesicles obtained by spraying: integrity of the vesicles. *Langmuir* **2005**, *21*, 7854−7859.
(10) Porcel, C. H.; Izquierdo, A.; Ball, V.; Decher, G.; Voegel, J.-C.; Schaaf, P. Ultrathin coatings and (poly(glutamic acid)/polyallylamine) films deposited by continuous and simultaneous spraying. *Langmuir* **2005**, *21*, 800−802.
(11) Mendelsohn, J. D.; Barrett, C. J.; Chan, V. V.; Pal, A. J.; Mayes, A. M.; Rubner, M. F. Fabrication of microporous thin films from polyelectrolyte multilayers. *Langmuir* **2000**, *16*, 5017−5023.
(12) Sukhorukov, G. B.; Mohwald, H.; Decher, G.; Lvov, Y. M. Assembly of polyelectrolyte multilayer films by consecutively alternating adsorption of polynucleotides and polycations. *Thin Solid Films* **1996**, *284−285*, 220−223.
(13) Lvov, Y.; Haas, H.; Decher, G.; Mohwald, H. Successive deposition of alternate layers of polyelectrolytes and a charged virus. *Langmuir* **1994**, *10*, 4232−4236.
(14) Fery, A.; Schler, B.; Cassagneau, T.; Caruso, F. Nanoporous thin films formed by salt-induced structural changes in multilayers of

poly(acrylic acid) and poly(allylamine). *Langmuir* **2001**, *17*, 3779−3783.
(15) Cassier, T.; Lowack, K.; Decher, G. Layer-by-layer assembled protein/polymer hybrid films: nanoconstruction via specific recognition. *Supramol. Sci.* **1998**, *5*, 309−315.
(16) Decher, G.; Lehr, B.; Lowack, K.; Lvov, Y.; Schmitt, J. New nanocomposite films for biosensors: layer-by-layer adsorbed films of polyelectrolytes, proteins or DNA. *Biosens. Bioelectron.* **1994**, *9*, 677−684.
(17) Lvov, Y.; Decher, G.; Sukhorukov, G. Assembly of thin films by means of successive deposition of alternate layers of DNA and poly(allylamine). *Macromolecules* **1993**, *26*, 5396−5399.
(18) Lang, J.; Liu, M. Layer-by-layer assembly of DNA films and their interactions with dyes. *J. Phys. Chem. B* **1999**, *103*, 11393−11397.
(19) Shi, X.; Sanedrin, R. J.; Zhou, F. Structural characterization of multilayered DNA and polylysine composite films: influence of ionic strength of DNA solutions on the extent of DNA incorporation. *J. Phys. Chem. B* **2002**, *106*, 1173−1180.
(20) Chen, X.; Lang, J.; Liu, M. Layer-by-layer assembly of DNA-dye complex films. *Thin Solid Films* **2002**, *409*, 227−232.
(21) Luo, L.; Liu, J.; Wang, Z.; Yang, X.; Dong, S.; Wang, E. Fabrication of layer-by-layer deposited multilayer films containing DNA and its interaction with methyl green. *Biophys. Chem.* **2001**, *94*, 11−22.
(22) Johnston, A. P. R.; Mitomo, H.; Read, E. S.; Caruso, F. Compositional and structural engineering of DNA multilayer films. *Langmuir* **2006**, *22*, 3251−3258.
(23) Yamauchi, F.; Koyamatsu, Y.; Kato, K.; Iwata, H. Layer-by-layer assembly of cationic lipid and plasmid DNA onto gold surface for stent-assisted gene transfer. *Biomaterials* **2006**, *27*, 3497−3504.
(24) Ishibashi, A.; Yamaguchi, Y.; Murakami, H.; Nakashima, N. Layer-by-layer assembly of RNA/single-walled carbon nanotube nanocomposites. *Chem. Phys. Let.* **2006**, *419*, 574−577.
(25) Qiu, X.; Leporatti, S.; Donath, E.; Mohwald, H. Studies on the drug release properties of polysaccharide multilayers encapsulated ibuprofen microparticles. *Langmuir* **2001**, *17*, 5375−5380.
(26) Serizawa, T.; Yamaguchi, M.; Akashi, M. Alternating bioactivity of polymeric layer-by-layer assemblies: anticoagulation vs procoagulation of human blood. *Biomacromolecules* **2002**, *3*, 724−731.
(27) Thierry, B.; Winnik, F. M.; Merhi, Y.; Silver, J.; Tabrizian, M. Bioactive coatings of endovascular stents based on polyelectrolyte multilayers. *Biomacromolecules* **2003**, *4*, 1564−1571.
(28) Shutava, T. G.; Lvov, Y. M. Nano-engineered microcapsules of tannic acid and chitosan for protein encapsulation. *J. Nanosci. Nanotechnol.* **2006**, *6*, 1655−1661.
(29) Stockton, W. B.; Rubner, M. F. Molecular-level processing of conjugated polymers. 4. Layer-by-layer manipulation of polyaniline via hydrogen-bonding interactions. *Macromolecules* **1997**, *30*, 2717−2725.
(30) Shimazaki, Y.; Mitsuishi, M.; Ito, S.; Yamamoto, M. Preparation of the layer-by-layer deposited ultrathin film based on the charge-transfer interaction. *Langmuir* **1997**, *13*, 1385−1387.
(31) Kamei, D.; Ajiro, H.; Hongo, C.; Akashi, M. Solvent effects on isotactic poly(methyl methacrylate) crystallization and syndiotactic poly(methacrylic acid) incorporation in porous thin films prepared by stepwise stereocomplex assembly. *Langmuir* **2009**, *25*, 280−285.
(32) Qiu, X.; Leporatti, S.; Donath, E.; Mohwald, H. Studies on the drug release properties of polysaccharide multilayers encapsulated ibuprofen microparticles. *Langmuir* **2001**, *17*, 5375−5380.
(33) Wang, L.; Wang, X.; Xu, M.; Chen, D.; Sun, J. Layer-by-layer assembled microgel films with high loading capacity: reversible loading and release of dyes and nanoparticles. *Langmuir* **2008**, *24*, 1902−1909.
(34) Park, M.-K.; Advincula, R. C. In-plane photoalignment of liquid crystals by azobenzene−polyelectrolyte layer-by-layer ultrathin films. *Langmuir* **2002**, *18*, 4532−4535.
(35) Yang, X.; Johnson, S.; Shi, J.; Holesinger, T.; Swanson, B. Polyelectrolyte and molecular host ion self-assembly to multilayer thin films: an approach to thin film chemical sensors. *Sens. Actuators, B* **1997**, *45*, 87−92.
(36) Ariga, K.; Vinu, A.; Ji, Q.; Ohmori, O.; Hill, J. P.; Acharya, S.; Koike, J.; Shiratori, S. A layered mesoporous carbon sensor based on nanopore-filling cooperative adsorption in the liquid phase. *Angew. Chem., Int. Ed.* **2008**, *47*, 7254−7257.
(37) Kim, J. H.; Kim, S. H.; Shiratori, S. Fabrication of nanoporous and hetero structure thin film via a layer-by-layer self assembly method for a gas sensor. *Sens. Actuators, B* **2004**, *102*, 241−247.
(38) Cho, J.; Hong, J.; Char, K.; Caruso, F. Nanoporous block copolymer micelle/micellea ultilayer films with dual optical properties. *J. Am. Chem. Soc.* **2006**, *128*, 9935−9942.
(39) Glinel, K.; Prevot, M.; Krustev, R.; Sukhorukov, G. B.; Jonas, A. M.; Mohwald, H. Control of the water permeability of polyelectrolytea ultilayers by deposition of charged paraffin particles. *Langmuir* **2004**, *20*, 4898−4902.
(40) Park, M.-K.; Deng, S.; Advincula, R. C. pH-sensitive bipolar ion-permselective ultrathin films. *J. Am. Chem. Soc.* **2004**, *126*, 13723−13731.
(41) Takenaka, S.; Maehara, Y.; Imai, H.; Yoshikawa, M.; Shiratori, S. Layer-by-layer self-assembly replication technique: application to photoelectrode of dye-sensitized solar cell. *Thin Solid Films* **2003**, *438*−*439*, 346−351.
(42) Fujita, S.; Shiratori, S. The optical properties of ultra-thin films fabricated by layer-by-layer adsorption process depending on dipping time. *Thin Solid Films* **2006**, *499*, 54−60.
(43) Nagaoka, Y.; Shiratori, S.; Einaga, Y. Photo-control of adhesion properties by detachment of the outermost layer in layer-by-layer assembled multilayerfilms of preyssler-type polyoxometalate and polyethyleneimine. *Chem. Mater.* **2008**, *20*, 4004−4010.
(44) Lvov, Y.; Ariga, K.; Onda, M.; Ichinose, I.; Kunitake, T. A careful examination of the adsorption step in the alternate layer-by-layer assembly of linear polyanion and polycation. *Colloids Surf., A* **1999**, *146*, 337−346.
(45) Sukhishvili, S. A.; Kharlampieva, E.; Izumrudov, V. A careful examination of the adsorption step in the alternate layer-by-layer assembly of linear polyanion and polycation. *Macromolecules* **2006**, *39*, 8873−8881.
(46) Shiratori, S.; Rubner, M. F. pH-dependent thickness behavior of sequentially adsorbed layers of weak polyelectrolytes. *Macromolecules* **2000**, *33*, 4213−4219.
(47) Caruso, F.; Caruso., R. A.; Mohwald, H. Nanoengineering of inorganic and hybrid hollow spheres by colloidal templating. *Science* **1998**, *282*, 1111−1114.
(48) Wong, J. E.; Richtering, W. Layer-by-layer assembly on stimuli-responsive microgels. *Curr. Opin. Colloid Interface Sci.* **2008**, *13*, 403−412.
(49) Manna, U.; Dhar, J.; Nayak, R.; Patil, S. Multilayer single-component thin films and microcapsules via covalent bonded layer-by-layer self-assembly. *Chem. Commun.* **2010**, *46*, 2250−2252.
(50) Huang, C.-J.; Chang, F.-C. Using click chemistry to fabricate ultrathin thermoresponsive microcapsules through direct covalent layer-by-layer assembly. *Macromolecules* **2009**, *42*, 5155−5166.
(51) Feng, Z.; Fan, G.; Wang, H.; Gao, C.; Shen, J. Polyphosphazene microcapsules fabricated through covalent assembly. *Macromol. Rapid Commun.* **2009**, *30*, 448−452.
(52) Tian, Y.; He, Q.; Tao, C.; Li, J. Fabrication of fluorescent nanotubes based on layer-by-layer assembly via covalent bond. *Langmuir* **2006**, *22*, 360−362.
(53) Kohli, P.; Blanchard, G. J. Applying polymer chemistry to interfaces: layer-by-layer and spontaneous growth of covalently bound multilayers. *Langmuir* **2000**, *16*, 4655−4661.
(54) Sun, Y.; Yan, F.; Yang, W.; Sun, C. Multilayered construction of glucose oxidase and silica nanoparticles on Au electrodes based on layer-by-layer covalent attachment. *Biomaterials* **2006**, *27*, 4042−4049.
(55) Such, G. K.; Quinn, J. F.; Quinn, A.; Tjipto, E.; Caruso, F. Assembly of ultrathin polymer multilayer films by click chemistry. *J. Am. Chem. Soc.* **2006**, *128*, 9318−9319.
(56) Rydzek, G.; Schaaf, P.; Voegel, J.-C.; Jierry, L.; Boulmedais, F. *Soft Matter* **2012**, *8*, 9738−9755.

(57) Chen, J.; Huang, L.; Ying, L.; Luo, G.; Zhao, X.; Cao, W. Self-assembly ultrathin films based on diazoresins. *Langmuir* **1999**, *15*, 7208−7212.
(58) Nomura, R.; Yamada., K.; Masuda, T. A chromophore-labeled poly(N-propargylamide): a new strategy for a stimuli-responsive conjugated polymer. *Chem. Commun.* **2002**, 478−479.
(59) Kang, Y. K.; Lee, O.-S.; Deria, P.; Kim, S. H.; Park, T.-H.; Bonnell, D. A.; Saven, J. G.; Therien, M. J. Helical wrapping of single-walled carbon nanotubes by water soluble poly(p-phenyleneethynylene). *Nano Lett.* **2009**, *9*, 1414−1418.
(60) Ferain, E.; Legras, R. Templates for engineered nano-objects for use in microwave, electronic devices and biomedical sensing application. *Nucl. Instrum. Methods Phys. Res., Sect. B* **2009**, *267*, 1028−1031.
(61) Terada, K.; Masuda, T.; Sanda, F. Synthesis and secondary structure of polyacetylenes carrying diketopiperazine moieties. The first example of helical polymers stabilized by s-cis-amide-based hydrogen bonding. *Macromolecules* **2009**, *42*, 913−920.
(62) Wang, Y.; Boysen, R. I.; Wood, B. R.; Kansiz, M.; McNaughton, D.; Hearn, M. T. W. Determination of the secondary structure of proteins in different environments by FTIR-ATR spectroscopy and PLS regression. *Biopolymers* **2008**, *89*, 895−905.
(63) Mori, T.; Kyotani, M.; Akagi, K. Helicity-controlled liquid crystal reaction field using nonbridged and bridged binaphthyl derivatives available for synthesis of helical conjugated polymers. *Macromolecules* **2008**, *41*, 607−613.
(64) Han, R.; Zwiefka., A.; Caswell., C. C.; Xu, Y.; Keene, D. R.; Lukomska, E.; Zhao, Z.; Höök, M.; Lukomski., S. Assessment of prokaryotic collagen-like sequences derived from streptococcal Scl1 and Scl2 proteins as a source of recombinant GXY polymers. *Appl. Microbiol. Biotechnol.* **2006**, *72*, 109−115.
(65) Boulmedais, F.; Schwinté, P.; Gergely, C.; Voegel, J.-C.; Schaaf, P. Secondary structure of polypeptide multilayer films: an example of locally ordered polyelectrolyte multilayers. *Langmuir* **2002**, *18*, 4523−4525.
(66) Boulmedais, F.; Bozonnet, M.; Schwinté, P.; Voegel, J.-C.; Schaaf, P. Multilayered polypeptide films: secondary structures and effect of various stresses. *Langmuir* **2003**, *19*, 9873−9882.
(67) Zhao, W.; Zheng, B.; Haynie, D. T. A molecular dynamics study of the physical basis of stability of polypeptide multilayer nanofilms. *Langmuir* **2006**, *22*, 6668−6675.
(68) Serizawa, T.; Hamada, K.; Kitayama, T.; Katsukawa, K.; Hatada, K.; Akashi, M. Stepwise assembly of isotactic poly(methyl methacrylate) and syndiotactic poly(methacrylic acid) on a substrate. *Langmuir* **2000**, *16*, 7112−7115.
(69) Matsukuma, D.; Aoyagi, T.; Serizawa, T. Adhesion of two physically contacting planar substrates coated with layer-by-layer assembled films. *Langmuir* **2009**, *25*, 9824−9830.
(70) Jaworek, T.; Neher, D.; Wegner, G.; Wieringa, R. H.; Schouten, A. J. Electromechanical properties of an ultrathin layer of directionally aligned helical polypeptides. *Science* **1998**, *279*, 57−60.
(71) Liscio, A.; Palermo, V.; Samorì, P. Nanoscale quantitative measurement of the potential of charged nanostructures by electrostatic and kelvin probe force microscopy: unraveling electronic processes in complex materials. *Acc. Chem. Res.* **2010**, *43*, 541−550.
(72) Nonnenmacher, M.; Oboyle, M. P.; Wickramasinghe, H. K. Kelvin probe force microscopy. *Appl. Phys. Lett.* **1991**, *58*, 2921−2923.
(73) Weaver, J. M. R.; Abraham, D. W. High resolution atomic force microscopy potentiometry. *J. Vac. Sci. Technol., B* **1991**, *9*, 1559−1561.
(74) Sasahara, A.; Hiehata, K.; Onishi, H. Metal-to-oxide charge transfer observed by a Kelvin probe force microscope. *Catal. Surv. Asia* **2009**, *13*, 9−15.
(75) Palermo, V.; Otten, M. B. J.; Liscio, A.; Schwartz, E.; de Witte, P. A. J.; Castriciano, M. A.; Wienk, M. M.; Nolde, F.; De Luca, G.; Cornelissen, J. J. L. M.; Janssen, R. A. J.; Müllen, K.; Rowan, A. E.; Nolte, R. J. M.; Samorì, P. The relationship between nanoscale architecture and function in photovoltaic multichromophoric arrays as visualized by Kelvin probe force microscopy. *J. Am. Chem. Soc.* **2008**, *130*, 14605−14614..
(76) Semenikhin, O. A.; Jiang, L.; Iyoda, T.; Hashimoto, K.; Fujishima, A. Atomic force microscopy and Kelvin probe force microscopy evidence of local structural inhomogeneity and nonuniform dopant distribution in conducting polybithiophene. *J. Phys. Chem.* **1996**, *100*, 18603−18606.
(77) Maturova, K.; Kemerink, M.; Wienk, M. M.; Charrier, D. S. H.; Janssen, R. A. J. Scanning Kelvin probe microscopy on bulk heterojunction polymer blends. *Adv. Funct. Mater.* **2009**, *19*, 1379−1386.
(78) Spadafora, E. J.; Demadrille, R.; Ratier, B.; Grévin, B. Imaging the carrier photogeneration in nanoscale phase segregated organic heterojunctions by Kelvin probe force microscopy. *Nano Lett.* **2010**, *10*, 3337−3342.
(79) Liu, L.; Li, G. Electrical characterization of single-walled carbon nanotubes in organic solar cells by Kelvin probe force microscopy. *Appl. Phys. Lett.* **2010**, *96*, 083302.
(80) Richards, D. N.; Zemlyanov, D. Y.; Asrar, R. M.; Chokshi, Y. Y.; Cook, E. M.; Hinton, T. J.; Lu, X.; Nguyen, V. Q.; Patel, N. K.; Usher, J. R.; Vaidyanathan, S.; Yeung, D. A.; Ivanisevic, A. DNA immobilization on GaP(100) investigated by Kelvin probe force microscopy. *J. Phys. Chem. C* **2010**, *114*, 15486−15490.
(81) Xu, D.-M.; Zhang, K.-D.; Wu, W.-J. Synthesis and characterization of stearyl-group-terminated dendrimers and thermosensitivity of their toluene solutions. *J. Appl. Polym. Sci.* **2005**, *98*, 341−346.
(82) Shuler, R. L.; Zisma, W. A. A study of films of poly(7-methyl L-glutamate) adsorbed on water using wave damping and other methods. *Macromolecules* **1972**, *5*, 487−492.
(83) Yakel, H. L., Jr. An X-ray diffraction investigation of poly-ε-carbobenzoxy-L-lysine and a complex form of poly-γ-methyl-L-glutamate. *Acta Crystallogr.* **1953**, *6*, 724−727.
(84) Zhang, J.; Senger, B.; Vautier, D.; Picart, C.; Schaaf, P.; Voegel, J.-C.; Lavalle, P. Natural polyelectrolyte films based on layer-by-layer deposition of collagen and hyaluronic acid. *Biomaterials* **2005**, *26*, 3353−3361.
(85) Feldötö, Z.; Varga, I.; Blomberg, E. Influence of salt and rinsing protocol on the structure of PAH/PSS polyelectrolyte multilayers. *Langmuir* **2010**, *26*, 17048−17057.
(86) Dressick, W. J.; Wahl, K. J.; Bassim, N. D.; Stroud, R. M.; Petrovykh, D. Y. Divalent−anion salt effects in polyelectrolyte multilayer depositions. *Langmuir* **2012**, *28*, 15831−15843.